

Radiation effects on microstructure and EPR signal of yttrium oxide rods

This content has been downloaded from IOPscience. Please scroll down to see the full text.

2017 IOP Conf. Ser.: Mater. Sci. Eng. 169 012009

(<http://iopscience.iop.org/1757-899X/169/1/012009>)

View [the table of contents for this issue](#), or go to the [journal homepage](#) for more

Download details:

IP Address: 179.228.251.238

This content was downloaded on 21/02/2017 at 15:01

Please note that [terms and conditions apply](#).

You may also be interested in:

[A Theoretical Study of the Effect of Eu ion Dopant on the Electronic Excitations of Yttrium Oxide and Yttrium Oxy-Sulphide](#)

Agalya Govindasamy, Chen Lv, Hideyuki Tsuboi et al.

[Radiation effects on TL and EPR of sodalite and application to dosimetry](#)

N F Cano, S Watanabe, A R Blak et al.

[EPR study of radiation-induced defects in the thermoluminescence dating medium zircon \(ZrSiO₄\)](#)

M A Laruhin, H J van Es, G R Bulka et al.

[A proposed method for retrospective eye dose assessments for the purposes of resolving cataract compensation claims](#)

Colette J Jeffery, Simon M Clark, Trevor R Pinks et al.

[Feasibility of reading LiF thermoluminescent dosimeters by electron spin resonance](#)

S L Breen and J J Battista

[An experimental and Monte Carlo investigation of the energy dependence of alanine/EPR dosimetry](#)

G G Zeng, M R McEwen, D W O Rogers et al.

[Modern trends and development in high-dose luminescent measurements](#)

V Kortov

[Enhancement of radiation effects by bismuth oxide nanoparticles for kilovoltage x-ray beams: A dosimetric study using a novel multi-compartment 3D radiochromic dosimeter](#)

M Alqathami, A Blencowe, U J Yeo et al.

Radiation effects on microstructure and EPR signal of yttrium oxide rods

S C Santos, O Jr Rodrigues , L L Campos

Instituto de Pesquisas Energeticas e Nucleares – IPEN, Av. Prof. Lineu Prestes 2242, Cidade Universitaria, Sao Paulo, Brazil.

silas.cardoso@usp.br

Abstract. Designing nanostructured materials with high dosimetric efficiency is a great challenge in radiation dosimetry research. From rare-earth series, yttrium oxide is considered as excellent host matrix for rare-earth ions, leading to formation of advanced functional materials with optical, mechanical, chemical, and thermal properties notably improved. Nevertheless, there is a lack of information which correlates microstructural characteristics and performance of rare earths. This work aims to evaluate the radiation effects on microstructure and EPR signal of Y_2O_3 rods produced by colloidal processing followed by sintering at $1600^\circ C/4h$ in air. Ceramic rods were exposed to gamma radiation with doses up to $100kGy$. Microstructural and dosimetric characterizations were performed by XRD, SEM and EPR techniques. Yttrium oxide rods as sintered exhibited dense microstructure (96.6% theoretical density) and linear EPR dose response behaviour for wide dose range. These results reveal that yttrium oxide is a promising material for radiation dosimetry.

1. Introduction

Innovation in design of dosimetric materials comprises synthesis, processing and conformation of nanostructured components. In addition, the properties of solid dosimetric materials depend on chemical composition, crystal lattice and microstructure, which is the arrangement of the atoms, phases and defects within a material.

The interaction of ionizing radiation (α , β , γ rays) with a solid can induce physical modifications such as excitation (ionization) of atoms and molecules, a pair of electron- hole that leads either recombination luminescence centres or to formation of an interstitial atom and vacancy. A powerful technique for characterization of ionizing induced defects is Electron Paramagnetic Resonance (EPR). In addition, EPR is used to evaluate polymerization reactions^[1], catalysis^[2], laser^[3], free radicals in living tissues and fluids^[4] and drug detection^[5]. EPR is a useful technique for solid state dosimetry.

Yttrium oxide (Y_2O_3) belongs to rare earth sesquioxides series and exhibits remarkable properties, which make it a promising material for radiation dosimetry. Further, Y_2O_3 applications include sintering aid^[6], catalysis^[7], luminescence^[8], electrical^[9], electronic^[10], mechanical^[11] and thermal^[12] materials. Even though Y_2O_3 presents great applicability, there is a lack of investigations on radiation effects in yttrium oxide based ceramics. The purpose of this paper is to evaluate radiation induced effects on microstructure evolution and EPR response of yttrium oxide rods produced by colloidal processing.



2. Experimental

For this work, yttrium oxide powders (Y_2O_3 99.99%; Johnson Matthey) with mean particle size (d_{50}) of 190nm, specific surface area (SSM) of $6.4m^2.g^{-1}$, pycnometric density (ρ) of $4.85g.cm^{-3}$ were used as raw material. Yttrium oxide rods were formed by colloidal processing using suspensions with 30vol% of Y_2O_3 particles prepared at pH 10 through tetramethylammonium hydroxide solution (TMAH, 25wt.% in water, Sigma Aldrich). All procedures and parameters for stabilization of Y_2O_3 suspensions are reported in our previous study^[13]. The homogenization of ceramic suspensions was performed with a ball mill for 24h using alumina spheres ($\phi_{spheres}=10mm$). Ceramic samples (4.35 x 2.27mm, height x diameter) were shaped as micro rods by casting using organic templates on a plaster plate as illustrated in Figure 1. Thermal treatment of conformed samples was realized in a vertical furnace (Lindberg Blue) at temperature of 1600°C for 4h in ambient atmosphere. Crystalline structure of as sintered samples was evaluated by X-ray diffraction (XRD; Rigaku Multiflex), scanning at $1^\circ.min^{-1}$, $\Delta\theta = 10-80^\circ(2\theta)$, radiation Cu- $k\alpha$ and identified according to powder diffraction files (PDF).

Batches of four yttrium oxide rods as sintered were irradiated with gamma source with doses from 1Gy to 100kGy in ambient temperature. Microstructural evaluation of irradiated samples was performed by Scanning electron microscopy (SEM, Inact-X Oxford). Crystal defects and radicals induced by ionizing radiation were characterized by electron paramagnetic resonance at ambient temperature and atmosphere using X-band EPR spectrometer (Bruker EMX PLUS). EPR spectra of samples were recorded using the following parameters: field modulation frequency of 100kHz, microwave power of 0.6325mW, center field at 3200G, sweep width of 6000 G, modulation amplitude of 4 G, time constant of 0.01ms and, 10 scans. The EPR spectra of irradiated samples were determined as a mean of each batch normalized by mean mass of samples. EPR dose response and time decay curves were plotted considering the mean of peak-peak amplitudes of irradiated samples.

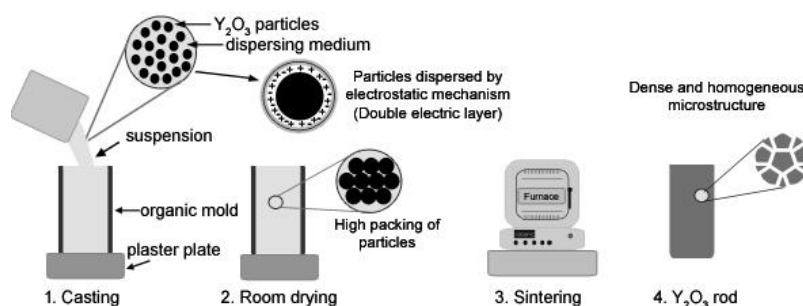


Figure 1 – Sequential colloidal processing for production of yttrium oxide rods.

3. Results and discussion

In ceramic processing there is a great concern on material structure, which has a profound effect on properties as well as on performance of the final product. The first type of structure is at atomic scale i.e. type of bonding and crystal structure (arrangement of atoms). Thus, crystal characterization is primordial step to development advanced materials for radiation dosimetry. Fig.2a shows XRD pattern of Y_2O_3 rods (Fig.2b). A characteristic diffraction peak of high intensity at 29° is observed, which is related with the crystallographic plane (222), corresponding to body-centered cubic yttria (C-type) and fitting the PDF (70-603) standard. Hoekstra et al.^[14] reported that rare earths sesquioxides belong to C-type as Dy_2O_3 , Th_2O_3 , Ga_2O_3 and In_2O_3 . In addition, literature has shown that Y_2O_3 can present other polymorphs. Gourlaouen et al.^[15] reported the monoclinic structure (B-type) at $997^\circ C$ under 2.0 GPa during plasma spray coating. Navrotsky et al.^[16] showed that the C-type becomes fluorite type at $2308^\circ C$ and hexagonal A-type at $2325^\circ C$. Quin et al.^[17] observed for particles smaller than 10nm structural changes of yttria from C-type to B-type.

The second type of structure refers to a larger scale and is a result of fabrication method. Microstructure concerns to the quantity and distribution of the structural elements/phases in a ceramic material and determines its properties such as ionic/electric conductivity, mechanical/chemical strength, abrasion resistance, and luminescence. Microstructural formation of ceramic rods shaped by colloidal processing is shown in Fig.3. Yttrium oxide powders have as characteristic flakey particles, forming agglomerates higher than $1\mu m$ (Fig.3a₁). A suitable stability condition for yttrium particles and homogenization of ceramic suspensions led to formation

of high compacted powders (Fig.3.a₂). The void space is eliminated by high temperature heat treatment, which results in densification of ceramic component. As shown in Fig.3a₃, as sintered yttrium oxide rods exhibited coarsened microstructure with rounded grains with size higher than 1µm.

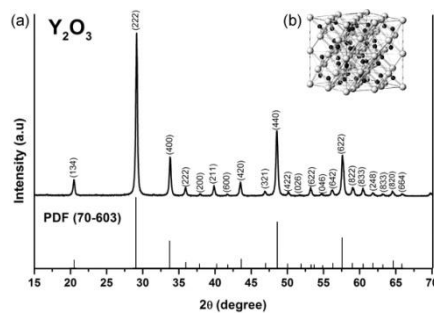


Figure 2. Crystal characterization of Y₂O₃ powders; (a) XRD curves of cubic C-type Y₂O₃; (b) model representation of crystal lattice of cubic C-type - dark spheres represent yttrium (Y) atoms and light ones oxygen (O) atoms.

Densification of a powder compact can be summarized using a model of two touching particles^[22], as shown in Fig.3. Initially neck growth dominates any mass transport between particles by grain boundary diffusion (Fig.3b) i.e. particle mass diffuses along the grain boundary to the surface to form a neck and as a consequence produces shrinkage (b₁-b₂). Besides, the mass transport still continues due to the differential size of the two grains. The smaller grain donates its mass to the larger one, which reduces the surface to volume ratio. Furthermore, although neck growth ceases the two sintered grains can reduce their free energy if the grain boundary moves through the smaller grain and disappears (b₂- b₃ and b₃-b₄). Kellet at al.^[23] reported that it is achieved via coarsening where the energy barrier for grain boundary motion is zero. In the case where the smaller particle is between two larger ones (Fig. 3c) the same sequential mass transport occurs i.e sintering (c₁-c₂)> grain boundary diffusion (c₂-c₃) > sintering (c₃-c₄). Besides, it is seen that the two larger grains touch one another (c₃), initiate grain growth and reinitiate shrinkage (c₃-c₄).

Fig.4a. shows SEM image of yttrium oxide rod sintered at 1600°C for 4h at ambient atmosphere. As can be seen, as sintered ceramic samples exhibited dense microstructure (Fig.4b), grain size larger than 1µm, pycnometric density of 4.84g.cm⁻³, which corresponds to 96,61% of theoretical density. From fracture micrograph (Fig.4c), is observed that ceramic rods exhibited dense microstructure with a closed pore situated within grain boundaries, as well as revealing transgranular fracture and cleavage planes, as indicated by white arrows.

Irradiation of materials with particles that are substantially energetic can produce atomic displacements, as well as can induce significant microstructural alteration. In contrast, gamma irradiation with doses up to 100kGy did not create microstructural changes for yttrium oxide rods. It is supposed to be ascribed to high energy bonding between Y-O atoms and the intrinsic properties of this rare earth sesquioxide. Light dots observed on grains surface (Fig.4d) are likely to be an approach of two sintered grains to reduce their free energy by moving from smaller grain to larger one.

EPR spectrum of Y₂O₃ rods irradiated with doses up to 100kGy at room atmosphere and temperature are shown in Fig. 5. As it can be seen, all samples exhibited EPR signal with an isotropic g tensor of 2.00 (c₁) and line width around 23G. The main defect c₁ is ascribed to interstitial O₂⁻ ion, nominally addressed as superoxide ion, which is generated by adsorption of molecular oxygen as observed by Lunsford^[24]. Osada et al^[25] reported these interstitial O₂⁻ ions in a study on Y₂O₃-CaO system, with tensor value g of 2.003. Singh et. al^[26] observed that for Y₂O₃:Er powders, EPR spectra exhibited as characteristic an axially g tensor with principal values g_{||} of 2.0415 and g_⊥ of 2.0056. The low intensity centre (c₂) illustrated in Fig. 5 exhibits smaller width line around 13G and g tensor of 1.969. The present center is assigned to F⁺ centre charged oxygen vacancy having one remaining electron. Besides, C-type crystal lattice of Y₂O₃ presents intrinsic oxygen vacancies which can produce F centres close to c₂. The effect of this point defect on luminescence of Y₂O₃ thins was discussed previously by Bordun^[27]. According to his study, thermal treatment of Y₂O₃ samples in air atmosphere leads to the filling the oxygen vacancies by oxygen atoms from air into Y₂O₃ and as a result, additional weak bonds with oxygen ions are formed. On irradiation a radiative recombination between these new centres and those intrinsic

centres occurs, resulting in an increase of the luminescence near 2.9eV. Singh et al.^[26] evaluated the stability of signal c_2 as a function of temperature and observed that this centre decays at low temperature around 180°C.

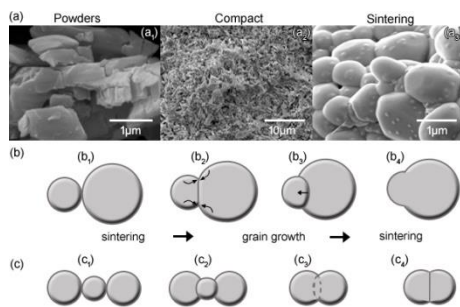


Figure 3. Sequential forming of yttrium oxide rods: (a) colloidal processing, (b) two touching particles; (c) two larger particles sandwiching a smaller particle

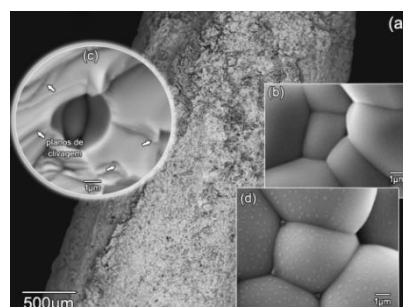


Figure 4. SEM images of Y_2O_3 rods sintered at 1600°C for 4h at room atmosphere, (a) ceramic rod as produced; (b) surface microstructure of unirradiated sample; (c) fracture surface, exhibiting cleavage planes in transgranular fracture (d) surface microstructure of gamma irradiated sample with 100kGy.

Fading behavior of dosimetric signal (c_1) of irradiated Y_2O_3 rods with doses up to 100kGy is illustrated in Fig. 6b. As can be seen, considering all doses the EPR relative signal of c_1 exhibited a mean decay of 23% until 96h after irradiation. Apart from this time, it became linear, revealing stability. Shivaramu et al.^[31] reported that yttria samples irradiated with 6kGy gamma dose exhibited up to 22% fading over a period of sixty days.

Dose dependence of any material is the fundamental basis of its application as a dosimetric material. Within the dose range of interest the response is expected to be reproducible as a function of dose and preferably linear. Linearity describes proportionality between EPR signal and absorbed dose. Usually, the dose response behavior of most dosimetric materials exhibits linear, supralinear and saturating response.

In this work, the EPR signal as a function of gamma radiation absorbed dose, determined as peak height of the main center (c_1), exhibited linear behavior up to 10kGy and presented a tendency of supralinearity for higher doses, as illustrated in Fig. 6a. Considering that a wide range of dose was evaluated, which was from 0,001 to 100kGy the plot scale was set to log-log in order to make visible the linearity of signal for lower doses.

Supralinearity refers to a region in which the slope of the response versus dose is greater than that for the linear region^[28]. Chen et al.^[29] described supralinearity as a property of the measured dose being above the continuation of the initial linear dose range. Furthermore, even if it is not related to this result, supralinearity may be ascribed to accumulation of doses, which can produce trapped electrons and holes at existing impurities along with the defects produced by the process of irradiation itself. As can be seen, Y_2O_3 rods present effective sensitivity for high dose radiation range. Salah et al.^[30] as evaluating dosimetric properties of $CaSO_4:Dy$ powders observed that particles in nano scale range were more sensitive, exhibiting a linear dose response behavior for high doses. Authors suggest that this behavior and supralinearity for nanocrystalline $CaSO_4:Dy$ might be related to the probability of formation of more numbers of traps, in which a large amount of particles are exposed directly to irradiation. As a consequence, the traps will compete to fill up the electronic levels while generating or while recombining during stimulation and finally, the supralinearity will occur if there is no much retrapping.

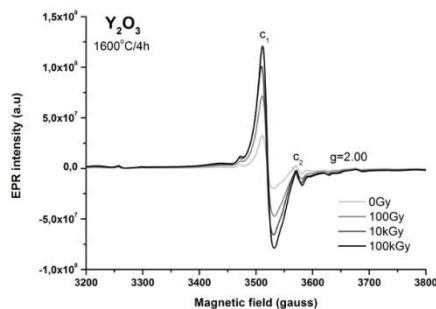


Figure 5 – EPR spectra recorded at room temperature and atmosphere for Y_2O_3 rods irradiated with doses up to 100kGy.

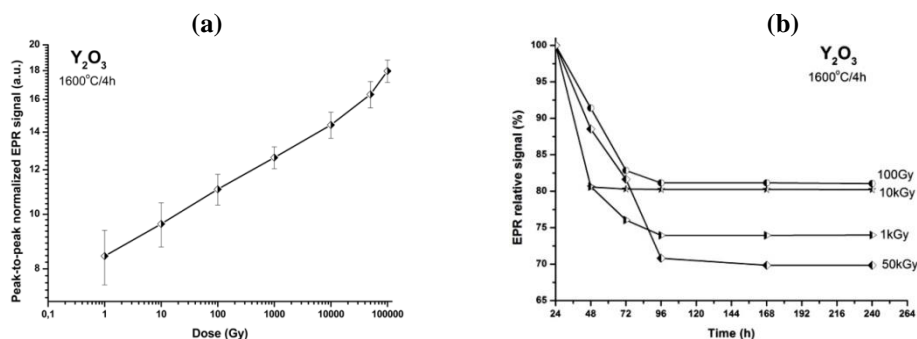


Figure 6 – (a) Peak-to-peak normalized EPR dose response of Y_2O_3 rods gamma irradiated with up to 100kGy ; (b) fading of Y_2O_3 rods at room temperature evaluated over 11 days

4. Conclusion

The effects of ionizing radiation on microstructure and electronic defects of yttrium oxide rods produced by colloidal processing followed by sintering at 1600°C for 4h in room atmosphere were evaluated. Ceramic samples exhibited dense microstructure and pycnometric density of 96.6%. None radiation induced defects were observed on microstructure of samples. However, for all samples EPR characterization revealed spectra with principal g tensor of 2.00 and maximum line width around 23G, which is ascribed to superoxide O_2^- ion generated by adsorption of molecular oxygen from room atmosphere. Dose response behaviour was linear from 0,1 to 10kGy range and supralinearity was observed for higher doses. Fading stability was achieved from 96h. The present results suggest that yttrium oxide is a promising material for high dose dosimetry applications.

5. Acknowledgments

We authors are deeply grateful to MSc. Douglas Will Leite, MSc. William Naville, and Dr. Masao Matsuoka. In addition, grant #2014/23621-3, São Paulo Research Foundation (FAPESP); National Council for Scientific and Technological Development (CNPq); and Coordination for Improvement of High Degree People (CAPES).

6. References

- [1] F.F. Li, L.Q. Xiao, L.J. Liu, Polymeric palladium-mediated carbene polymerization, *Polym Chem-Uk*, 6 (2015) 6163-6170.
- [2] R.R. Cheng, Z.L. Wu, Y.L. Hou, J. Dong, J.Z. Cui, B. Zhao, Three Cu(II) coordination polymers with novel bi-triazole ligand: Synthesis, structure and EPR properties, *Inorg Chem Commun*, 51 (2015) 95-98.
- [3] N.E. Domracheva, V.E. Vorobeve, M.S. Gruzdev, A.V. Pyataev, Blue shift in optical absorption, magnetism and light-induced superparamagnetism in gamma-Fe₂O₃ nanoparticles formed in dendrimer, *J Nanopart Res*, 17 (2015).

- [4] M. Hashem, M. Weiler-Sagie, P. Kuppusamy, G. Neufeld, M. Neeman, A. Blank, Electron spin resonance microscopic imaging of oxygen concentration in cancer spheroids, *J Magn Reson*, 256 (2015) 77-85.
- [5] M.A. Morsy, A.N.M. Kawde, Electron paramagnetic resonance monitoring for on-demand electrochemically-generated radicals, *Electrochim Acta*, 160 (2015) 22-27.
- [6] M. Marina, M.Z.M. Zamzuri, M.N. Derman, M.A. Selamat, Z. Nooraizedfiza, Comparison Study in Consolidation of Yttria Reinforced Iron-Chromium Composites using Conventional and Microwave Sintering Technique, *Advanced Materials Engineering and Technology Ii*, 594-595 (2014) 832-836.
- [7] F. Hayashi, M. Tanaka, D.M. Lin, M. Iwamoto, Surface structure of yttrium-modified ceria catalysts and reaction pathways from ethanol to propene, *J Catal*, 316 (2014) 112-120.
- [8] X.M. Han, X. Feng, X.W. Qi, X.Q. Wang, M.Y. Li, The Photoluminescent Properties of $Y_2O_3:Bi^{3+}, Eu^{3+}, Dy^{3+}$ Phosphors for White-Light-Emitting Diodes, *J Nanosci Nanotechno*, 14 (2014) 3387-3390.
- [9] A. Jyotsana, G.S. Maurya, A.K. Srivastava, A.K. Rai, B.K. Ghosh, Synthesis and electrical properties of $Y_2O_3: Dy^{3+} & Eu^{3+}$ nanoparticles, *Appl Phys a-Mater*, 117 (2014) 1269-1274.
- [10] T. Mongstad, A. Thogersen, A. Subrahmanyam, S. Karazhanov, The electronic state of thin films of yttrium, yttrium hydrides and yttrium oxide, *Sol Energ Mat Sol C*, 128 (2014) 270-274.
- [11] M.A. Auger, V. de Castro, T. Leguey, J. Tarcisio-Costa, M.A. Monge, A. Munoz, R. Pareja, Effect of yttrium addition on the microstructure and mechanical properties of ODS RAF steels, *J Nucl Mater*, 455 (2014) 600-604.
- [12] J. Hostasa, J. Matejicek, B. Nait-Ali, D.S. Smith, W. Pabst, L. Esposito, Thermal Properties of Transparent Yb-Doped YAG Ceramics at Elevated Temperatures, *J Am Ceram Soc*, 97 (2014) 2602-2606.
- [13] S.C. Santos, W. Acchar, C. Yamagata, S. Mello-Castanho, Yttria nettings by colloidal processing, *J Eur Ceram Soc*, 34 (2014) 2509-2517.
- [14] H.R. Hoekstra, K.A. Gingerich, High-Pressure B-Type Polymorphs of Some Rare-Earth Sesquioxides, *Science*, 146 (1964) 1163-&.
- [15] V. Gourlaouen, G. Schnedecker, A.M. Lejus, M. Boncoeur, R. Collongues, Metastable Phases in Yttrium-Oxide Plasma Spray Deposits and Their Effect on Coating Properties, *Mater Res Bull*, 28 (1993) 415-425.
- [16] A. Navrotsky, L. Benoist, H. Lefebvre, Direct calorimetric measurement of enthalpies of phase transitions at 2000 degrees-2400 degrees C in yttria and zirconia, *J Am Ceram Soc*, 88 (2005) 2942-2944.
- [17] X. Qin, Y.G. Ju, S. Bernhard, N. Yao, Flame synthesis of $Y_2O_3 : Eu$ nanophosphors using ethanol as precursor solvents, *J Mater Res*, 20 (2005) 2960-2968.
- [18] M.F. Yan, Effects of physical, chemical, and kinetic factors on ceramic sintering, in: K.S.M. G.L. Messing, J.W. McCauley, R. A. Haber (Ed.) *Advanced Ceramics*, American Ceramic Society, Westerville, OH, 1987.
- [19] M.A. Yar, S. Wahlberg, M.O. Abuelnaga, M. Johnsson, M. Muhammed, Processing and sintering of yttrium-doped tungsten oxide nanopowders to tungsten-based composites, *J Mater Sci*, 49 (2014) 5703-5713.
- [20] X.B. Li, Q.Q. Zhang, S.Y. Ma, G.X. Wan, F.M. Li, X.L. Xu, Microstructure optimization and gas sensing improvement of ZnO spherical structure through yttrium doping, *Sensor Actuat B-Chem*, 195 (2014) 526-533.
- [21] V. Kumar, O.P. Pandey, K. Singh, K. Lu, Interaction Study of Yttria-Based Glasses with High-Temperature Electrolyte for SOFC, *Fuel Cells*, 14 (2014) 635-644.
- [22] F.F. Lange, B.J. Kellett*, Thermodynamics of Densification: II, Grain Growth in Porous Compacts and Relation to Densification, *J Am Ceram Soc*, 72 (1989) 735-741.
- [23] B.J. Kellett, F.F. Lange, Thermodynamics of Densification: I, Sintering of Simple Particle Arrays, Equilibrium Configurations, Pore Stability, and Shrinkage, *J Am Ceram Soc*, 72 (1989) 725-734.
- [24] J.H. Lunsford, ESR of Adsorbed Oxygen Species, *Catal Rev*, 8 (1973) 135-157.
- [25] Y. Osada, S. Koike, T. Fukushima, S. Ogasawara, T. Shikada, T. Ikariya, Oxidative Coupling of Methane over Y_2O_3 -Cao Catalysts, *Appl Catal*, 59 (1990) 59-74.
- [26] V. Singh, V.K. Rai, I. Ledoux-Rak, S. Watanabe, T.K.G. Rao, J.F.D. Chubaci, L. Badie, F. Pelle, S. Ivanova, NIR to visible up-conversion, infrared luminescence, thermoluminescence and defect centres in $Y_2O_3 : Er$ phosphor, *J Phys D Appl Phys*, 42 (2009).
- [27] O.M. Bordun, Influence of Oxygen Vacancies on the Luminescence Spectra of Y_2O_3 Thin Films, *J Appl Spectrosc+*, 69 (2002) 430-433.
- [28] A. Standard, Standard practice for use of thermoluminescence dosimetry (TLD) systems for radiation processing, 2005.
- [29] R. Chen, S.W.S. Mckeever, Characterization of Nonlinearities in the Dose Dependence of Thermoluminescence, *Radiat Meas*, 23 (1994) 667-673.
- [30] N. Salah, P.D. Sahare, S.P. Lochab, P. Kumar, TL and PL studies on $CaSO_4: Dy$ nanoparticles, *Radiat Meas*, 41 (2006) 40-47.

[31] N.J. Shivaramu, B.N. Lakshminarasappa, K.R. Nagabhushana, F. Singh, Synthesis characterization and luminescence studies of gamma irradiated nanocrystalline yttrium oxide, *Spectrochim Acta A*, 154 (2016) 220-231.